

# 000 001 002 003 004 005 006 007 008 009 010 011 012 013 014 015 016 017 018 019 020 021 022 023 024 025 026 027 028 029 030 031 032 033 034 035 036 037 038 039 040 041 042 043 044 045 046 047 048 049 050 051 052 053 UNICoD: ENHANCING ROBOT POLICY VIA UNI-FIED CONTINUOUS AND DISCRETE REPRESENTATION LEARNING

Anonymous authors

Paper under double-blind review

## ABSTRACT

Building generalist robot policies that can handle diverse tasks in open-ended environments is a central challenge in robotics. To leverage knowledge from large-scale pretraining, prior work has typically built generalist policies either on top of vision-language understanding models (VLMs) or generative models. However, both semantic understanding from vision-language pretraining and visual dynamics modeling from visual-generation pretraining are crucial for embodied robots. Recent unified models of generation and understanding have demonstrated strong capabilities in both comprehension and generation through large-scale pretraining. We posit that robotic policy learning can likewise benefit from the combined strengths of understanding, planning and continuous future representation learning. Building on this insight, we introduce UniCoD, which acquires the ability to dynamically model high-dimensional visual features through pretraining on over 1M internet-scale instructional manipulation videos. Subsequently, UniCoD is fine-tuned on data collected from the robot embodiment, enabling the learning of mappings from predictive representations to action tokens. Extensive experiments show our approach consistently outperforms baseline methods in terms of 9% and 12% across simulation environments and real-world out-of-distribution tasks. Demos and code can be found at our anonymous website.

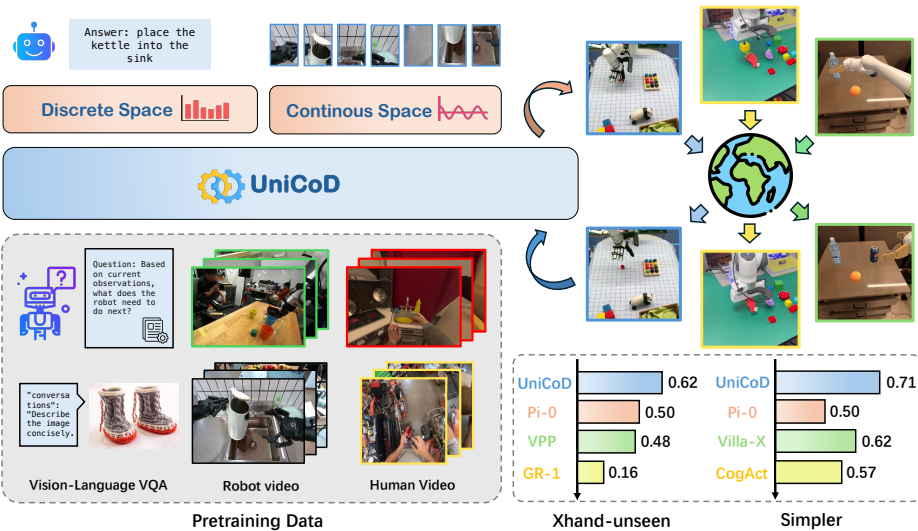


Figure 1: **Overview of UniCoD.** Our proposed UniCoD, which utilizes both understanding and prediction tasks under discrete and continuous representation space, demonstrates strong semantic generalization capabilities on real-world manipulation tasks, particularly in its ability to handle completely novel objects not seen during training. The upper right displays benchmark evaluations across several simulations and 2 real-world robots.

054 

## 1 INTRODUCTION

055  
 056 Constructing generalist foundation models (Zitkovich et al., 2023; Kim et al., 2024b) for robots  
 057 manipulation in the physical world has emerged as a rapidly growing frontier within embodied AI.  
 058 Vision–language–action (VLA) models aim to learn robotic policies from data annotated with vision,  
 059 linguistic, and action signals. However, the scarcity of robotic data and the heterogeneity across  
 060 embodiments present substantial challenges, particularly in achieving generalization to novel scenes  
 061 and task instructions, and in accurately predicting actions.

062 To mitigate these limitations, recent studies have explored mapping Vision–Language Models (VLMs)  
 063 into the action space(Black et al., 2024; Team et al., 2024). This strategy provides robot policies with  
 064 alignment priors across language and vision modalities. Nevertheless, these approaches often overlook  
 065 the fundamental discrepancies between robotic action tasks and vision–language tasks. Unlike the  
 066 abundance of internet-scale vision–language data, fine-tuning VLMs on limited robotic datasets  
 067 frequently leads to degradation of their foundational capabilities (Xing et al., 2025). Complementary  
 068 lines of work have investigated leveraging generation models as intermediaries for action policy  
 069 learning(Hu et al., 2024; Wen et al., 2024). While such visual foresight approaches facilitate dynamic  
 070 representation learning and enable the use of heterogeneous data sources, they typically fail to  
 071 preserve vision–language alignment inherent to pretrained VLMs. These observations highlight a  
 072 central insight: it is crucial to design robot-specific post-training paradigms tailored to embodied  
 073 scenarios. Upon re-examining this line of approaches, we observe that both language understanding  
 074 and future state prediction can provide preliminary guidance for general manipulation tasks. The  
 075 unified learning strategy further enables the model to acquire representations beneficial for robotic  
 076 tasks from a broader range of data.

077 Building upon these insights and prior advances in vision–language–action (VLA) research(Zhang  
 078 et al., 2025; Wang et al., 2025b), we propose UniCoD, which follows an understand-  
 079 ing–generation–execution paradigm that integrates discrete task comprehension with continuous  
 080 prediction of future robotic states. To address heterogeneous modalities, UniCoD employs a MOT  
 081 architecture (Liang et al., 2024) with modality-specialized experts. UniCoD is trained in two stages  
 082 to introduce continuous feature forecasting to action learning while maintaining general capabilities  
 083 within VLM. In the first stage, we curate and label a diverse collection of Embodied QA data sourced  
 084 from both robots(Khazatsky et al., 2024; Bu et al., 2025; Wu et al., 2024) and human demon-  
 085 strations(Hoque et al., 2025; Grauman et al., 2022). We enable the model to learn discrete language  
 086 representations for understanding of embodied scenes and continuous visual representations for world  
 087 modeling. In the second stage, we introduce embodiment-specific robotic data annotated with action  
 088 behaviors. By jointly predicting continuous visual futures and actions, the model learns to utilize  
 089 semantically aligned features that are rich in dynamic information. This, in turn, equips the VLA  
 090 policy with better generalization capabilities for new objects and scenes.

091 In experiments, UniCoD achieves a 9% improvement in the Simpler benchmark compared to existing  
 092 SOTA approach and demonstrates strong semantic generalization for real-world robots for complex  
 093 tasks on both robot arms and dexterous hands. In summary, our contributions are as follows:

- 094 • We propose a novel vision–language–action (VLA) that integrates both discrete and continuous  
 095 representations for understanding and learning dynamics, which is pre-trained on large-scale data  
 096 from both robot and human demonstrations, enabling effective transfer to embodied tasks.
- 097 • We propose a two-stage training framework that aligns action representations while preserving the  
 098 aligned intermediate representations.
- 099 • Our best-performing model achieves state-of-the-art results across both simulated and real-world  
 100 environments, and we further analyze the impact of different feature design choices on the model’s  
 101 capabilities.

102 

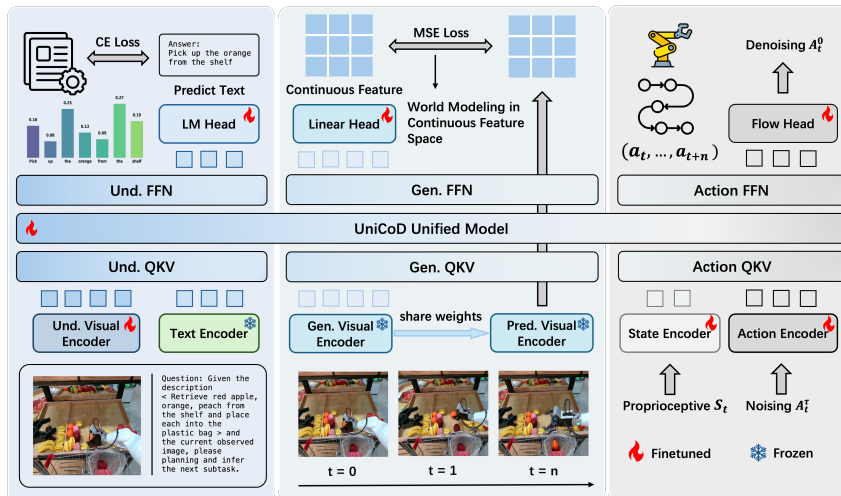
## 2 RELATED WORKS

103 **Vision-Language-Action Models** Vision-Language-Action (VLA) models introduce multimodal  
 104 large language models (Dai et al., 2024; Touvron et al., 2023; Wang et al., 2025a; Bai et al., 2025)  
 105 into robot policy models to enhance their generalization ability (Brohan et al., 2023; Kim et al.,  
 106 2024a; Black et al., 2024; Guo et al., 2025). This line of work either utilizes the VLM and an

108 action head for end-to-end action prediction (Li et al., 2023; Wen et al., 2025) or uses the VLM  
 109 to extract key information to condition downstream policy (Zhang et al., 2024; Li et al., 2025).  
 110 Some recent works have introduced additional auxiliary tasks to VLAs, including enhancing spatial  
 111 understanding (Qu et al., 2025), QA reasoning (Zhou et al., 2025), visual reasoning (Zhao et al.,  
 112 2025) and prediction (Zhang et al., 2025), demonstrating that both general-purpose understanding and  
 113 generation capabilities can promote action learning. However, these methods are primarily limited to  
 114 unifying generative tasks within a discrete token prediction framework, which may compromise the  
 115 robust vision-language alignment inherent in the pre-trained VLM. In this work, we incorporate a  
 116 continuous-space visual prediction task to aid downstream action learning.  
 117

118 **Generalist Robot Policies with Joint Prediction** Explorations into generalist robot policies have  
 119 considered using world models (Blattmann et al., 2023; Assran et al., 2025; Chen et al., 2024; Guo  
 120 et al., 2024) to learn physical dynamics and subsequently predict actions (Du et al., 2024; Black et al.,  
 121 2023). Many recent methods have incorporated prediction into larger-scale data and models: GR-1  
 122 (Wu et al., 2023) utilizes video pre-training to initialize the action policy; VPP (Hu et al., 2024) uses  
 123 a video foundation model as the visual encoder for action policy. While these methods fully leverage  
 124 the rich information from video data, they lack semantic grounding capabilities due to the absence of  
 125 large language models. Recent works (Zhang et al., 2025; Wang et al., 2025b) use VQ quantization  
 126 to incorporate predictive generation tasks into VLA policies, demonstrating the potential for unifying  
 127 understanding and prediction. In contrast, we utilize continuous visual features as the prediction  
 128 supervision signal and pre-train our model on large-scale language prediction and continuous visual  
 129 prediction tasks.  
 130

### 131 3 METHODOLOGY



151 **Figure 2: Illustration of the UniCoD framework.** UniCoD adopts a MoT framework to handle  
 152 text understanding and planning, continuous visual prediction, and action execution. The continuous  
 153 features are derived from future observations using a frozen vision encoder.  
 154

155 In this section, we present the overall framework design and the two-stage training strategy of UniCoD,  
 156 as illustrated in Figure 2. In the first stage, UniCoD is trained to learn joint text–image representations  
 157 across diverse manipulation datasets, including understanding, planning, and continuous future  
 158 prediction tasks. In the subsequent stage, an action expert is employed to integrate the multimodal  
 159 inputs and predicted future states with action. In the subsequent subsections, we will respectively  
 160 describe: (1) the joint visual-language embedding learning for pre-training in Sec 3.1, (2) our policy  
 161 learning method in Sec 3.2, and (3) the implementation details and training data in Sec 3.3.

162  
163

## 3.1 UNIFIED VISION LANGUAGE JOINT EMBEDDING MODELING

164  
165  
166  
167  
168  
169  
170

Before introducing the robot action space, we first establish a cross-embodiment pre-training paradigm for robots. In this stage, a subset of the model parameters  $U_{v,l}$  is jointly optimized via the Text-Image to Embedding(TI2E) (examples can be found in A.5). Concretely, given a language instruction  $l$  and the current view observations  $o_t$  at time  $t$ , UniCoD is trained to predict the joint visual–text embedding:  $\hat{o}_{t+h}, \hat{l} = U_{v,l}(o_t, l)$ , where  $\hat{o}_{t+h} = V(o_{t+h}) = \{c_1, c_2, \dots, c_n\}$  denotes the predicted continuous future representation encoded by the visual encoder  $V$ , while  $\hat{l} = \{d_1, d_2, \dots, d_m\}$  corresponds to the  $m$ -token textual sequence.

171  
172  
173  
174  
175  
176

**Discrete Representation Learning.** To enhance vision–language alignment, the parameters  $U_{v,l}$  are initialized from a pre-trained vision–language model. Fine-grained language representations are derived from large-scale vision–language datasets, as well as planning and scene descriptions from embodied tasks, which are annotated using pre-trained MLLM into a VQA-style format. This target enables the agent to gain a better understanding of diverse instructions and scenes, thereby facilitating the learning of continuous representations for visual prediction and action.

177  
178  
179  
180  
181  
182

**World Modeling under Continuous Space.** In the pre-training stage, to acquire dynamic representations associated with the action space, we introduce additional attention weights dedicated to future state prediction, which are integrated with the original VLM within the mixture-of-transformers framework. Unlike prior approaches that directly predict image pixels, we leverage a frozen visual encoder to represent future observations in a continuous high-dimensional space, capturing high-level information across different semantics. A more detailed discussion can be found in Appendix A.1.

183  
184  
185  
186  
187

For the visual inputs, we employ a dual-encoder design that combines the VLM visual encoder with a generator encoder. The tokens generated by the latter are processed by the generative expert in the mixture-of-transformers and, together with the language tokens and VLM visual tokens, jointly participate in the attention computation. This design preserves the pretrained model’s vision–language alignment while enabling the prediction process to benefit from richer semantic understanding.

188  
189  
190  
191  
192  
193

**Training Objective.** The visual and language inputs are processed respectively through the MoT framework, then autoregressively generate  $\hat{o}_{t+h}^{pred} = d_{1:m}^{pred}$ , while the generation expert obtains the  $\hat{o}_{t+h}^{pred} = c_{1:n}^{pred}$ . We follow the standard setup of generative–understanding models, employing cross-entropy loss for the language branch and mean squared error loss for the generative branch. This optimaze progress can be formulated as:

194  
195  
196

$$\mathcal{L}_1 = \lambda_1 \cdot \frac{1}{n} \sum_{i=1}^n \left\| c_i^{pred} - c_i \right\|_2^2 - (1 - \lambda_1) \cdot \frac{1}{m} \sum_{j=1}^m \log P_\theta(d_j | d_{<j}, l, o_t) \quad (1)$$

197  
198

where  $\lambda_1$  serves as a weighting factor to balance the loss contributions of the discrete and continuous representations.

199  
200

## 3.2 UNIFIED ACTION MODELING

201  
202  
203  
204  
205  
206

In the previous stage, we obtained  $U_{v,l}$  through pre-training, which endowed the model with basic capabilities in future state prediction and vision–language alignment. However,  $U_{v,l}$  cannot yet be directly mapped to the action space. To address this limitation, in the second stage we fine-tune  $U_{v,l}$  on embodiment data comprising visual, language, and action modalities, while simultaneously training an action expert from scratch to construct  $U_{v,l,a}$ .

207  
208  
209  
210  
211  
212  
213

**Action & State Expert.** Similar to the generation and understanding experts, we employ distinct attention weights to project actions and states (i.e., proprioception) into a shared attention space. Unlike the other experts, the action expert leverages flow matching to capture the continuous and inherently multi-modal distribution of the action space. Proprioceptive signals  $s_t$  are processed by an MLP-based state expert encoder, enabling fusion within the unified model. Given an action sequence  $A_t = (a_t, a_{t+1}, \dots, a_{t+h})$  to be executed, along with the observation  $o_t$  and instruction  $l$ , the unified model  $U_{v,l,a}$  is trained to approximate vector fields as:

214  
215

$$\mathcal{L}_{flow} = \mathbb{E}_{\tau \sim \mathcal{U}(0,1)} \mathbb{E}_{\{A_t, o_t, s_t, l\} \sim \mathcal{D}} \left[ \left\| U_{v,l,a}(A_t^\tau, o_t, s_t, l, \tau) - (A_t - A_t^\tau) \right\|_2^2 \right], \quad (2)$$

where  $A_t^\tau = (1 - \tau)\epsilon + \tau A_t$  denotes the interpolated actions at step  $\tau$ , and  $\epsilon \sim \mathcal{N}(0, I)$ .

216 In this action training stage, we also jointly optimize the generation expert by predicting the future  
 217 observation states  $c_{1:n}$ , yielding the following objective:  
 218

$$219 \quad \mathcal{L}_2 = \lambda_2 \cdot \frac{1}{n} \sum_{i=1}^n \left\| c_i^{\text{pred}} - c_i \right\|_2^2 + (1 - \lambda_2) \mathcal{L}_{\text{flow}}. \quad (3)$$

### 222 3.3 IMPLEMENTATION DETAILS

224 **Model Setting.** UniCoD employs Paligemma Beyer et al. (2024) as the VLM expert. For future  
 225 observation encoding, we experiment with SigLIP Tschanen et al. (2025), DINOv3 Siméoni et al.  
 226 (2025), and direct pixel-level prediction. Considering the information flow across modalities, we  
 227 adopt a block-wise masking mechanism in the MoT attention: within each modality, bidirectional  
 228 attention is applied, while across modalities a causal mask is enforced following the order of image,  
 229 language, image prediction, state information, and action.

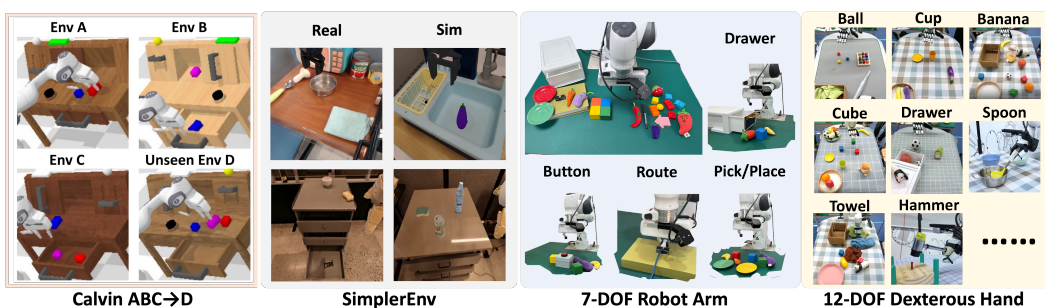
230 **Pre-training Data.** In the pretraining stage, we utilize three categories of data to acquire joint  
 231 text-image representations: (1) 320k robot videos paired with fine-grained subtask descriptions and  
 232 overall task instructions, which yield VQA and TI2E data for the generation-understanding task; (2)  
 233 870k robot and human operation videos accompanied by task instructions, which are used as TI2E  
 234 data; and (3) 560k generic vision-language question answering data, employed for co-training to  
 235 preserve the fundamental capabilities of the VLM. In the action modeling stage, we exclusively adopt  
 236 VLA data collected in both simulation and real-world robotic environments. Further details regarding  
 237 the datasets are provided in Appendix A.5.

## 238 4 EXPERIMENT

240 To comprehensively evaluate our proposed method, UniCoD, we conduct extensive experiments  
 241 across two simulation benchmarks and on two distinct real-world robotic platforms. Our experiments  
 242 are designed to assess the performance of UniCoD and validate the effectiveness of our proposed  
 243 modules.

### 245 4.1 EXPERIMENTAL SETUP

247 Our experiments are conducted and deployed across four distinct environments. Figure 3 illustrates a  
 248 selection of tasks from both our simulation and real-world settings.



261 Figure 3: Our evaluation environments, including 2 simulation benchmarks and 2 real-world embodi-  
 262 ments.

263 **Calvin Benchmark** Calvin is a simulation benchmark designed for evaluating long-horizon,  
 264 language-conditioned manipulation policies. We employ the *ABC-D* split to evaluate the single-view  
 265 generalization capabilities of the models. The evaluation suite includes 1,000 long-horizon sequences,  
 266 each of length 5. We report the average length of completed sub-task sequences.

267 **SimplerEnv Benchmark** SimplerEnv is a simulation benchmark designed to evaluate policies  
 268 trained on real-world datasets, such as Bridge-V2 and Fractal. The benchmark supports two types of  
 269 robot arms: WindowX and Google Robot. For our evaluation, we conduct 240 runs for each task and  
 report the average success rate.

270 **Real-World Franka Emika Panda Arm** We deploy models on a Franka Emika arm for real-world  
 271 task comparison. We first collected a dataset of 2,000 trajectories spanning over 20 distinct tasks,  
 272 encompassing six fundamental skills: picking, placing, opening a drawer, closing a drawer, pressing  
 273 a button, and routing a cable. We evaluate performance on both seen and unseen task variations.  
 274 The unseen category primarily involves grasping novel objects not present in the training data and  
 275 introducing misleading objects. More details can be found in Appendix A.3.1.

276 **Real-World XArm with 12-DOF X-Hand** On our dexterous manipulation platform, we train  
 277 different models using a dataset of 4,000 trajectories across more than 100 tasks. The models are  
 278 then evaluated in a variety of seen and unseen scenarios, which cover 13 distinct skills in 9 categories.  
 279 More details can be found in Appendix A.3.2.

## 281 4.2 SIMULATION EXPERIMENTS

283 **Implementation Details** We first pre-train UniCoD following the methodology described in Sec-  
 284 tion 3. Subsequently, we fine-tune the model on 8 A100 GPUs for 22k steps, using a learning rate  
 285 of  $5 \times 10^{-5}$  and a batch size of 1024. For all simulation training, we consistently use a single,  
 286 third-person-view image of size  $224 \times 224$  as the visual input. In Calvin, we use an action chunk  
 287 size of 10, and during deployment, the full 10-step chunk is executed at each inference step. In  
 288 SimplerEnv, we use an action chunk size of 4; for the WindowX environment (corresponding to  
 289 the Bridge dataset), the full 4-step chunk is executed, whereas for the Google Robot environment  
 290 (corresponding to the Fractal dataset), half of the action chunk is executed.

291 **Baselines** We compare UniCoD against several state-of-the-art VLAs and prediction-based policies.  
 292 On SimplerEnv, we benchmark UniCoD against RT-1-X (Brohan et al., 2022), Octo (Team et al.,  
 293 2024), OpenVLA (Kim et al., 2024a), RoboVLMs (Liu et al., 2025), SpatialVLA (Qu et al., 2025),  
 294  $\pi_0$  (Black et al., 2024), CogAct (Li et al., 2024) and Villa-x (Chen et al., 2025). On Calvin, we  
 295 compare UniCoD against several policies that leverage visual generation tasks, including GR-1 (Wu  
 296 et al., 2023),  $\pi_0$  (Black et al., 2024), VPP (Hu et al., 2024), and UP-VLA (Zhang et al., 2025). To  
 297 ensure a fair comparison, we reproduce these baselines and standardize their visual input to a single  
 298 third-person view. For  $\pi_0$ , we specifically use the implementation from the open-pi-zero and report its  
 299 performance under the same training and evaluation setup used in UniCoD for a direct comparison.

### 300 4.2.1 PERFORMANCE ON SIMULATION BENCHMARKS

303 Table 1: Results on SimplerEnv-WindowsX (visual matching). Entries marked with \* are methods  
 304 reproduced with our training and test settings.

306 <b>Model</b>	307 Carrot on Plate		308 Eggplant in Basket		309 Spoon on Towel		310 Stack Cube		311 Success
	312 <b>Grasp</b>	313 <b>Success</b>	314 <b>Grasp</b>	315 <b>Success</b>	316 <b>Grasp</b>	317 <b>Success</b>	318 <b>Grasp</b>	319 <b>Success</b>	
320 RT-1-X	321 20.8	322 4.2	323 0.0	324 0.0	325 16.7	326 0.0	327 8.3	328 0.0	329 1.1
330 Octo-Base	331 52.8	332 8.3	333 66.7	334 43.1	335 34.7	336 12.5	337 31.9	338 0.0	339 16.0
340 OpenVLA	341 33.3	342 0.0	343 8.3	344 4.1	345 4.1	346 0.0	347 12.5	348 0.0	349 1.0
350 RoboVLMs	351 33.3	352 20.8	353 91.7	354 79.2	355 70.8	356 45.8	357 54.2	358 4.2	359 37.5
360 SpatialVLA	361 29.2	362 25.0	363 100.0	364 <b>100.0</b>	365 20.8	366 16.7	367 62.5	368 29.2	369 42.7
370 $\pi_0^*$	371 58.5	372 48.8	373 78.8	374 64.6	375 83.3	376 73.3	377 62.5	378 12.5	379 49.8
380 CogAct	381 /	382 <b>58.3</b>	383 /	384 45.8	385 /	386 29.2	387 /	388 <b>95.8</b>	389 57.3
390 Villa-x	391 /	392 46.3	393 /	394 64.6	395 /	396 77.9	397 /	398 61.3	399 <b>62.5</b>
400 UniCoD (Ours)	401 75.0	402 <b>63.0</b>	403 100.0	404 <b>89.6</b>	405 83.3	406 <b>78.8</b>	407 91.7	408 52.5	409 <b>71.0</b>

316  
 317 Tables 1 and 3 present the performance of our method on the SimplerEnv-WindowX and SimplerEnv-  
 318 Google Robot benchmarks, respectively. We report the officially published results of other methods  
 319 for comparison. On both robotic platforms, our method achieves the highest success rates of 71.0%  
 320 and 78.4%, attaining state-of-the-art (SOTA) performance. We highlight the top-performing and  
 321 second-best methods for each task category in **bold** and with an underline. It is evident that UniCoD  
 322 demonstrates consistently high success rates across all sub-tasks. This contrasts with other methods,  
 323 which often exhibit “spiky” performance profiles—excelling on some tasks while performing poorly  
 324 on others. This finding underscores the superior multi-task learning capabilities of our approach.

324 Furthermore, for a fair, apple-to-apple comparison with the architecturally similar  $\pi_0$  baseline, we  
 325 reproduced it within our identical training and evaluation framework. Across both environments, we  
 326 found that the novel components in UniCoD yield a significant performance uplift of over 20%. We  
 327 also observed that this improvement is consistently present at every training checkpoint, indicating  
 328 that the stable gains can be attributed to our method’s ability to learn continuous future features and  
 329 discrete representations simultaneously.

330 We also compare UniCoD against several policies that leverage advanced  
 331 vision-based training methodologies on the Calvin ABC-D split, with  
 332 results shown in Table 2. Since  
 333 many prior works utilize multi-view  
 334 images and historical information,  
 335 we re-implemented these baselines  
 336 using a standardized single, third-  
 337 person-view image as visual input  
 338 to ensure a fair comparison of the  
 339 benefits conferred by our training  
 340 method. The results demonstrate  
 341 that UniCoD achieves the best performance on single-view manipulation tasks within  
 342 the Calvin benchmark. Moreover, when compared to the baseline  $\pi_0$ , our method  
 343 again exhibits a performance improvement, consistent with the results on SimplerEnv.  
 344

### 345 4.3 REAL WORLD EXPERIMENTS

348 **Implementation Details** We fine-tune  
 349 the pre-trained UniCoD model separately  
 350 on the datasets collected from our two  
 351 real-world robotic platforms to evaluate its  
 352 performance on a variety of seen and un-  
 353 seen tasks. The fine-tuning process is  
 354 conducted for 10 epochs using a batch size  
 355 of 1024 and a learning rate of  $5 \times 10^{-5}$ ,  
 356 with both the prediction horizon and ac-  
 357 tion chunk length set to 10. For the Franka  
 358 Emika Panda arm, the model is fine-tuned  
 359 on 2,000 trajectories, and during deploy-  
 360 ment, we evaluate both full and half action  
 361 chunk execution, reporting the superior result. On the XArm with a 12-DOF dexterous hand, we use  
 362 a larger dataset of 4,000 trajectories and execute the full 10-step action chunk at each inference step.  
 363 We test on seen tasks, which involve familiar objects in novel, randomized positions, and un-  
 364 seen tasks, which introduce novel color, objects, and background. For each task configuration, we conduct  
 365 20 trials from randomized initial configurations and report the average task success rate. More details  
 366 can be found in Appendix A.3.

#### 367 4.3.1 PERFORMANCE ON REAL WORLD EXPERIMENTS

368 We compare UniCoD against OpenVLA(Kim et al., 2024a), GR-1 (Wu et al., 2023),  $\pi_0$  (Black et al.,  
 369 2024), UP-VLA (Zhang et al., 2025) and VPP (Hu et al., 2024) in two environments, visualizing  
 370 the results in Figure 4 and 5. Our method achieves the highest overall task success rates on  
 371 both real-world robotic platforms. Specifically, on the Franka Panda arm, UniCoD attains the best  
 372 performance across all four task categories, outperforming baselines on both seen and un-  
 373 seen tasks. This demonstrates that our approach effectively enhances both multi-task learning and generalization  
 374 capabilities. Consistent with our findings in the Simpler simulation environment, our method again  
 375 shows superior performance over the architecturally similar  $\pi_0$  baseline across a majority of these  
 376 real-world tasks. Furthermore, on the more complex 12-DoF dexterous hand platform, UniCoD  
 377 achieves the highest average success rate across all nine skill categories. Notably, we observe that our  
 378 method exhibits a significant generalization advantage when dealing with novel objects and scenes.

Table 2: Long-horizon evaluation on the Calvin ABC→D benchmark. Entries marked with \* are methods reproduced with our training and test settings. We *only use a single 224x224 third-view image* as input in all methods.

Method	Tasks completed in a row					Avg. Len ↑
	1	2	3	4	5	
RT-1*	0.533	0.222	0.094	0.038	0.013	0.900
GR-1	0.854	0.712	0.596	0.497	0.401	3.06
$\pi_0$ *	0.937	0.832	0.740	0.629	0.510	3.65
VPP*	0.909	0.815	0.713	0.620	0.518	3.58
UP-VLA*	0.928	0.865	0.815	0.769	0.699	4.08
UniCoD (Ours)	0.973	0.895	0.823	0.752	0.670	4.11

379 The results demonstrate that UniCoD achieves the best performance on single-view manipulation tasks within  
 380 the Calvin benchmark. Moreover, when compared to the baseline  $\pi_0$ , our method  
 381 again exhibits a performance improvement, consistent with the results on SimplerEnv.

Table 3: Results on SimplerEnv-Google Robot (visual  
 382 matching). Entries marked with \* are methods repro-  
 383 duced with our training and test settings.

Model	Pick Coke	Move Near	O.C. Drawer	Put in Drawer	AVG↑
RT-1-X	56.7	31.7	59.7	21.3	42.4
Octo-Base	17.0	4.2	22.7	0.0	11.0
OpenVLA	16.3	46.2	35.6	0.0	24.5
RoboVLMs	77.3	61.7	43.5	24.1	51.7
$\pi_0$ *	93.3	78.1	23.6	12.5	51.9
CogACT	91.3	<b>85.0</b>	<b>71.8</b>	50.9	<b>74.8</b>
Villa-x	<b>98.7</b>	75.0	59.3	5.6	59.6
UniCoD (Ours)	<b>98.7</b>	<b>81.5</b>	<b>63.2</b>	<b>70.0</b>	<b>78.4</b>

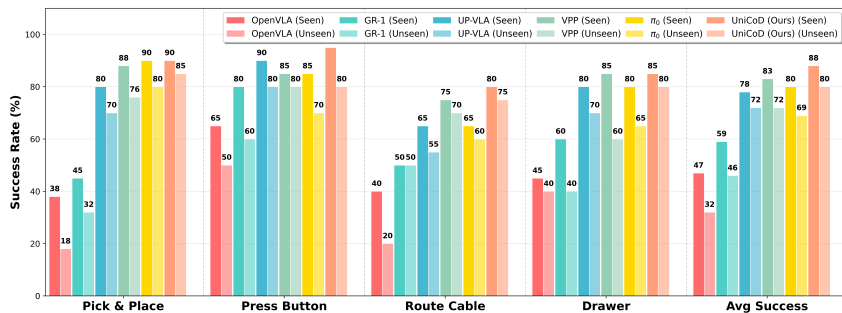


Figure 4: Results on real-world 7DOF robotarm experiment. More detailed quantitative results are provided in Table 6.

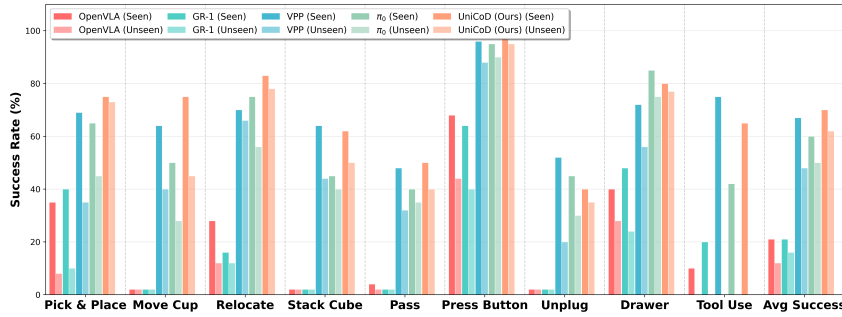


Figure 5: Results on real-world 12-DOF dexterous hands experiment. More detailed quantitative results can be found in Table 7.

We provide several illustrative examples in Appendix A.4, where the model successfully grasps completely unseen objects and correctly interprets out-of-distribution (OOD) language descriptions.

These consistent, state-of-the-art results across two morphologically distinct robots validate the effectiveness and broad applicability of our proposed method.

#### 4.4 ABLATION STUDY

In this section, we conduct a series of ablation studies to validate the effectiveness of the different components within UniCoD. These experiments investigate the role of our continuous visual representations, the impact of our large-scale pre-training phase involving both language and visual prediction, and a comparison of several continuous vision encoding methods proposed in Sec 3. All ablation studies are conducted in the Simpler simulation environment, following the same training and evaluation protocols described in Sec 4.2.

#### Effectiveness of Continuous Prediction

**Visual Representations** To validate the effectiveness of prediction using continuous representations, we compare a version of UniCoD without pre-training against two baselines, as shown in Table 4. We evaluate the following without using pretraining: (1) w/o Continuous ( $\pi_0$ ), where the modules for predicting continuous future features (including the auxiliary prediction expert and its corresponding encoder/decoder) are removed. (2) w/Pred, which predicts future raw pixels using a two-layer MLP. This helps us elucidate the trade-offs between using high-level visual features versus raw pixels

Table 4: Ablation study on unified pretraining paradigm and continuous feature for prediction.

Model	Carrot	Eggplant	Spoon	Cube	AVG↑
w/o Pretrain					
w/o Continuous	48.8	64.6	73.3	12.5	49.8
w/o Continuous w/ Pred	52.5	79.2	79.6	30.0	60.3
UniCoD	60.8	87.1	78.8	50.4	69.3
w/ Pretrain					
UniCoD (Ours)	<b>63.0</b>	<b>89.6</b>	<b>78.8</b>	<b>52.5</b>	<b>71.0</b>

432 as the predictive signal. The results in w/o Pretrain section of the table show that our proposed  
 433 continuous visual feature prediction boosts performance by approximately 20%. Furthermore, the  
 434 comparison with w/Pred reveals that continuous features are indeed a more effective signal for  
 435 future prediction, enabling the model to extract dynamic information crucial for action generation.  
 436

437 **Effectiveness of Large-Scale Planning and Prediction Pre-training** Table 4 also presents a  
 438 comparison between UniCoD with and without pre-training. Overall, pre-training improves the  
 439 success rate across all tasks, yielding a performance gain of approximately 2%. During fine-tuning,  
 440 we observe that leveraging large-scale external data for future and language prediction accelerates  
 441 the model’s convergence on the robotics dataset. This effect is particularly pronounced in the  
 442 convergence of the future prediction loss. This indicates that our joint pre-training scheme, which  
 443 combines continuous and discrete prediction, provides a superior model initialization, especially for  
 444 the prediction expert module, which translates to tangible benefits during downstream fine-tuning.  
 445

Method	Google robot					WidowX robot				
	Pick	Move	Drawer	Put	AVG	Carrot	Eggplant	Spoon	Cube	AVG
UniCoD-Distill	97.2	82.6	<b>61.9</b>	<b>74.4</b>	<b>79.0</b>	48.8	<b>95.8</b>	<b>89.6</b>	34.6	67.2
UniCoD-Dino	<b>98.3</b>	<b>80.2</b>	51.1	63.3	73.2	54.6	81.7	78.8	49.6	66.1
UniCoD-Siglip	97.7	80.2	61.3	72.4	77.9	<b>60.8</b>	87.1	78.8	<b>50.4</b>	<b>69.3</b>

451  
 452 Table 5: Ablation study on choice of continuous vision features.  
 453

454 **Choice of Continuous Visual Prediction** We further compare the different encoding methods for  
 455 future prediction proposed in our methodology. Specifically, we evaluate three distinct approaches (all  
 456 without pre-training), with results on both Simpler environments shown in Table 5: (1) UniCoD-Distill,  
 457 which takes the input embeddings of the ViT (from the current frame) as input to the prediction expert  
 458 and predicts the output features of ViT for the future frame. This approach is analogous to distilling  
 459 knowledge from the ViT encoder itself. (2) UniCoD-Dino and (3) UniCoD-Siglip, which take the  
 460 output features of their respective vision encoders (DINO Siméoni et al. (2025) or SigLIP Tschannen  
 461 et al. (2025)) for the current frame as input to predict the corresponding features for the future frame.  
 462 The results show that UniCoD-Siglip demonstrates better performance on both benchmarks, and  
 463 consequently, we select SigLIP as the vision encoder for our UniCoD model. Notably, on Google  
 464 Robot environment, UniCoD-Distill achieves better performance than the UniCoD-Siglip when  
 465 neither is pre-trained. This suggests that the distillation-style architecture has inherent advantages. In  
 466 contrast, UniCoD-Dino performs significantly worse than the other two. This is likely because the  
 467 DINO feature space is not aligned with the VLM backbone. Conversely, since SigLIP is the native  
 468 vision encoder for Paligemma, its feature space is naturally more aligned with that of the VLM expert,  
 469 facilitating more effective integration within the prediction expert.  
 470

## 5 CONCLUSION

471 In this paper, we introduce **UniCoD**, a Vision-Language-Action (VLA) framework that enhances  
 472 policy learning by integrating discrete token prediction with continuous visual prediction. During  
 473 the pre-training stage, we leverage embodied VQA and robotic planning tasks to align the discrete  
 474 language features of a Vision-Language Model (VLM). Concurrently, we train a predictive module  
 475 on large-scale video data to forecast future continuous visual features. These two components—the  
 476 VLM backbone and the prediction module—are effectively fused using a Mixture-of-Experts (MoE)  
 477 Transformer architecture. In the subsequent action fine-tuning stage, an action expert is incorporated,  
 478 and the entire model is fine-tuned on a joint objective of continuous action generation and future fea-  
 479 ture prediction. Our method achieves state-of-the-art (SOTA) performance in two distinct simulation  
 480 environments. Furthermore, on real-world hardware, including a 7-DoF robot arm and a 12-DoF  
 481 dexterous hand, our model demonstrates superior performance and stronger semantic generalization,  
 482 particularly when handling novel objects not encountered during training.  
 483  
 484  
 485

486 

## 6 ETHICS STATEMENT

487  
488 The data used in the VLM4VLA is sourced exclusively from public repositories. Our contributions  
489 fully adhere to the terms of these licenses. We did not use any data beyond what is publicly available  
490 and downloadable.  
491492 

## 7 REPRODUCIBILITY STATEMENT

493  
494 All results and experimental conclusions in this paper are reproducible. To facilitate reproducibility,  
495 we have included our source code in the supplementary material. We are committed to open science  
496 and plan to publicly release the complete codebase, trained models, datasets, and evaluation logs  
497 upon publication of this work.  
498500 

## REFERENCES

501  
502 Mido Assran, Adrien Bardes, David Fan, Quentin Garrido, Russell Howes, Matthew Muckley, Ammar  
503 Rizvi, Claire Roberts, Koustuv Sinha, Artem Zholus, et al. V-jepa 2: Self-supervised video models  
504 enable understanding, prediction and planning. *arXiv preprint arXiv:2506.09985*, 2025.  
505  
506 Shuai Bai, Keqin Chen, Xuejing Liu, Jialin Wang, Wenbin Ge, Sibo Song, Kai Dang, Peng Wang,  
507 Shijie Wang, Jun Tang, et al. Qwen2. 5-vl technical report. *arXiv preprint arXiv:2502.13923*,  
508 2025.  
509  
510 Lucas Beyer, Andreas Steiner, André Susano Pinto, Alexander Kolesnikov, Xiao Wang, Daniel  
511 Salz, Maxim Neumann, Ibrahim Alabdulmohsin, Michael Tschannen, Emanuele Bugliarello, et al.  
512 Paligemma: A versatile 3b vlm for transfer. *arXiv preprint arXiv:2407.07726*, 2024.  
513  
514 Kevin Black, Mitsuhiro Nakamoto, Pranav Atreya, Homer Walke, Chelsea Finn, Aviral Kumar, and  
515 Sergey Levine. Zero-shot robotic manipulation with pretrained image-editing diffusion models.  
516 *arXiv preprint arXiv:2310.10639*, 2023.  
517  
518 Kevin Black, Noah Brown, Danny Driess, Adnan Esmail, Michael Equi, Chelsea Finn, Niccolo Fusai,  
519 Lachy Groom, Karol Hausman, Brian Ichter, et al. pi\_0: A vision-language-action flow model for  
520 general robot control. *arXiv preprint arXiv:2410.24164*, 2024.  
521  
522 Andreas Blattmann, Tim Dockhorn, Sumith Kulal, Daniel Mendelevitch, Maciej Kilian, Dominik  
523 Lorenz, Yam Levi, Zion English, Vikram Voleti, Adam Letts, et al. Stable video diffusion: Scaling  
524 latent video diffusion models to large datasets. *arXiv preprint arXiv:2311.15127*, 2023.  
525  
526 Anthony Brohan, Noah Brown, Justice Carbajal, Yevgen Chebotar, Joseph Dabis, Chelsea Finn,  
527 Keerthana Gopalakrishnan, Karol Hausman, Alex Herzog, Jasmine Hsu, et al. Rt-1: Robotics  
528 transformer for real-world control at scale. *arXiv preprint arXiv:2212.06817*, 2022.  
529  
530 Anthony Brohan, Noah Brown, Justice Carbajal, Yevgen Chebotar, Xi Chen, Krzysztof Choromanski,  
531 Tianli Ding, Danny Driess, Avinava Dubey, Chelsea Finn, et al. Rt-2: Vision-language-action  
532 models transfer web knowledge to robotic control. *arXiv preprint arXiv:2307.15818*, 2023.  
533  
534 Qingwen Bu, Jisong Cai, Li Chen, Xiuqi Cui, Yan Ding, Siyuan Feng, Shenyuan Gao, Xindong  
535 He, Xuan Hu, Xu Huang, et al. Agibot world colosseo: A large-scale manipulation platform for  
536 scalable and intelligent embodied systems. *arXiv preprint arXiv:2503.06669*, 2025.  
537  
538 Xiaoyu Chen, Junliang Guo, Tianyu He, Chuheng Zhang, Pushi Zhang, Derek Cathera Yang, Li Zhao,  
539 and Jiang Bian. Igor: Image-goal representations are the atomic control units for foundation  
models in embodied ai, 2024. URL <https://arxiv.org/abs/2411.00785>.  
540  
541 Xiaoyu Chen, Hangxing Wei, Pushi Zhang, Chuheng Zhang, Kaixin Wang, Yanjiang Guo, Rushuai  
542 Yang, Yucen Wang, Xinquan Xiao, Li Zhao, et al. Villa-x: enhancing latent action modeling in  
543 vision-language-action models. *arXiv preprint arXiv:2507.23682*, 2025.

540 Gheorghe Comanici, Eric Bieber, Mike Schaeckermann, Ice Pasupat, Noveen Sachdeva, Inderjit  
 541 Dhillon, Marcel Blstein, Ori Ram, Dan Zhang, Evan Rosen, et al. Gemini 2.5: Pushing the frontier  
 542 with advanced reasoning, multimodality, long context, and next generation agentic capabilities.  
 543 *arXiv preprint arXiv:2507.06261*, 2025.

544 Wenliang Dai, Junnan Li, Dongxu Li, Anthony Meng Huat Tiong, Junqi Zhao, Weisheng Wang,  
 545 Boyang Li, Pascale N Fung, and Steven Hoi. Instructclip: Towards general-purpose vision-  
 546 language models with instruction tuning. *Advances in Neural Information Processing Systems*, 36,  
 547 2024.

548 Yilun Du, Sherry Yang, Bo Dai, Hanjun Dai, Ofir Nachum, Josh Tenenbaum, Dale Schuurmans, and  
 549 Pieter Abbeel. Learning universal policies via text-guided video generation. *Advances in Neural  
 550 Information Processing Systems*, 36, 2024.

552 Kristen Grauman, Andrew Westbury, Eugene Byrne, Zachary Chavis, Antonino Furnari, Rohit  
 553 Girdhar, Jackson Hamburger, Hao Jiang, Miao Liu, Xingyu Liu, et al. Ego4d: Around the world in  
 554 3,000 hours of egocentric video. In *Proceedings of the IEEE/CVF conference on computer vision  
 555 and pattern recognition*, pp. 18995–19012, 2022.

556 Yanjiang Guo, Yucheng Hu, Jianke Zhang, Yen-Jen Wang, Xiaoyu Chen, Chaochao Lu, and Jianyu  
 557 Chen. Prediction with action: Visual policy learning via joint denoising process. *arXiv preprint  
 558 arXiv:2411.18179*, 2024.

560 Yanjiang Guo, Jianke Zhang, Xiaoyu Chen, Xiang Ji, Yen-Jen Wang, Yucheng Hu, and Jianyu  
 561 Chen. Improving vision-language-action model with online reinforcement learning. *arXiv preprint  
 562 arXiv:2501.16664*, 2025.

563 Ryan Hoque, Peide Huang, David J Yoon, Mouli Sivapurapu, and Jian Zhang. Egodex: Learning  
 564 dexterous manipulation from large-scale egocentric video. *arXiv preprint arXiv:2505.11709*, 2025.

566 Yucheng Hu, Yanjiang Guo, Pengchao Wang, Xiaoyu Chen, Yen-Jen Wang, Jianke Zhang, Koushil  
 567 Sreenath, Chaochao Lu, and Jianyu Chen. Video prediction policy: A generalist robot policy with  
 568 predictive visual representations. *arXiv preprint arXiv:2412.14803*, 2024.

569 Tao Jiang, Tianyuan Yuan, Yicheng Liu, Chenhao Lu, Jianning Cui, Xiao Liu, Shuiqi Cheng, Jiyang  
 570 Gao, Huazhe Xu, and Hang Zhao. Galaxea open-world dataset and g0 dual-system vla model.  
 571 *arXiv preprint arXiv:2509.00576*, 2025.

573 Alexander Khazatsky, Karl Pertsch, Suraj Nair, Ashwin Balakrishna, Sudeep Dasari, Siddharth  
 574 Karamcheti, Soroush Nasiriany, Mohan Kumar Srirama, Lawrence Yunliang Chen, Kirsty Ellis,  
 575 et al. Droid: A large-scale in-the-wild robot manipulation dataset. *arXiv preprint arXiv:2403.12945*,  
 576 2024.

577 Moo Jin Kim, Karl Pertsch, Siddharth Karamcheti, Ted Xiao, Ashwin Balakrishna, Suraj Nair, Rafael  
 578 Rafailov, Ethan Foster, Grace Lam, Pannag Sanketi, Quan Vuong, Thomas Kollar, Benjamin  
 579 Burchfiel, Russ Tedrake, Dorsa Sadigh, Sergey Levine, Percy Liang, and Chelsea Finn. Openvla:  
 580 An open-source vision-language-action model. *arXiv preprint arXiv:2406.09246*, 2024a.

581 Moo Jin Kim, Karl Pertsch, Siddharth Karamcheti, Ted Xiao, Ashwin Balakrishna, Suraj Nair,  
 582 Rafael Rafailov, Ethan Foster, Grace Lam, Pannag Sanketi, et al. Openvla: An open-source  
 583 vision-language-action model. *arXiv preprint arXiv:2406.09246*, 2024b.

585 Peiyan Li, Yixiang Chen, Hongtao Wu, Xiao Ma, Xiangnan Wu, Yan Huang, Liang Wang, Tao Kong,  
 586 and Tieniu Tan. Bridgevla: Input-output alignment for efficient 3d manipulation learning with  
 587 vision-language models. *arXiv preprint arXiv:2506.07961*, 2025.

588 Qixiu Li, Yaobo Liang, Zeyu Wang, Lin Luo, Xi Chen, Mozheng Liao, Fangyun Wei, Yu Deng,  
 589 Sicheng Xu, Yizhong Zhang, et al. Cogact: A foundational vision-language-action model for  
 590 synergizing cognition and action in robotic manipulation. *arXiv preprint arXiv:2411.19650*, 2024.

591 Xinghang Li, Minghuan Liu, Hanbo Zhang, Cunjun Yu, Jie Xu, Hongtao Wu, Chilam Cheang,  
 592 Ya Jing, Weinan Zhang, Huaping Liu, et al. Vision-language foundation models as effective robot  
 593 imitators. *arXiv preprint arXiv:2311.01378*, 2023.

594 Weixin Liang, Lili Yu, Liang Luo, Srinivasan Iyer, Ning Dong, Chunting Zhou, Gargi Ghosh, Mike  
 595 Lewis, Wen-tau Yih, Luke Zettlemoyer, et al. Mixture-of-transformers: A sparse and scalable  
 596 architecture for multi-modal foundation models. *arXiv preprint arXiv:2411.04996*, 2024.

597

598 Haotian Liu, Chunyuan Li, Qingyang Wu, and Yong Jae Lee. Visual instruction tuning, 2023. URL  
 599 <https://arxiv.org/abs/2304.08485>.

600 Huaping Liu, Xinghang Li, Peiyan Li, Minghuan Liu, Dong Wang, Jirong Liu, Bingyi Kang, Xiao  
 601 Ma, Tao Kong, and Hanbo Zhang. Towards generalist robot policies: What matters in building  
 602 vision-language-action models. *arXiv preprint arXiv:2412.14058*, 2025.

603

604 Delin Qu, Haoming Song, Qizhi Chen, Yuanqi Yao, Xinyi Ye, Yan Ding, Zhigang Wang, JiaYuan Gu,  
 605 Bin Zhao, Dong Wang, et al. Spatialvla: Exploring spatial representations for visual-language-  
 606 action model. *arXiv preprint arXiv:2501.15830*, 2025.

607 Oriane Siméoni, Huy V Vo, Maximilian Seitzer, Federico Baldassarre, Maxime Oquab, Cijo Jose,  
 608 Vasil Khalidov, Marc Szafraniec, Seungeun Yi, Michaël Ramamonjisoa, et al. Dinov3. *arXiv  
 609 preprint arXiv:2508.10104*, 2025.

610

611 Octo Model Team, Dibya Ghosh, Homer Walke, Karl Pertsch, Kevin Black, Oier Mees, Sudeep  
 612 Dasari, Joey Hejna, Tobias Kreiman, Charles Xu, et al. Octo: An open-source generalist robot  
 613 policy. *arXiv preprint arXiv:2405.12213*, 2024.

614 Hugo Touvron, Thibaut Lavril, Gautier Izacard, Xavier Martinet, Marie-Anne Lachaux, Timothée  
 615 Lacroix, Baptiste Rozière, Naman Goyal, Eric Hambro, Faisal Azhar, et al. Llama: Open and  
 616 efficient foundation language models. *arXiv preprint arXiv:2302.13971*, 2023.

617 Michael Tschannen, Alexey Gritsenko, Xiao Wang, Muhammad Ferjad Naeem, Ibrahim Alabdul-  
 618 mohsin, Nikhil Parthasarathy, Talfan Evans, Lucas Beyer, Ye Xia, Basil Mustafa, et al. Siglip 2:  
 619 Multilingual vision-language encoders with improved semantic understanding, localization, and  
 620 dense features. *arXiv preprint arXiv:2502.14786*, 2025.

621

622 Homer Rich Walke, Kevin Black, Tony Z Zhao, Quan Vuong, Chongyi Zheng, Philippe Hansen-  
 623 Estruch, Andre Wang He, Vivek Myers, Moo Jin Kim, Max Du, et al. Bridgedata v2: A dataset for  
 624 robot learning at scale. In *Conference on Robot Learning*, pp. 1723–1736. PMLR, 2023.

625 Weiyun Wang, Zhangwei Gao, Lixin Gu, Hengjun Pu, Long Cui, Xingguang Wei, Zhaoyang Liu,  
 626 Linglin Jing, Shenglong Ye, Jie Shao, et al. Internvl3. 5: Advancing open-source multimodal  
 627 models in versatility, reasoning, and efficiency. *arXiv preprint arXiv:2508.18265*, 2025a.

628

629 Yuqi Wang, Xinghang Li, Wenxuan Wang, Junbo Zhang, Yingyan Li, Yuntao Chen, Xinlong Wang,  
 630 and Zhaoxiang Zhang. Unified vision-language-action model. *arXiv preprint arXiv:2506.19850*,  
 631 2025b.

632 Junjie Wen, Yichen Zhu, Jinming Li, Zhibin Tang, Chaomin Shen, and Feifei Feng. Dexvla:  
 633 Vision-language model with plug-in diffusion expert for general robot control. *arXiv preprint  
 634 arXiv:2502.05855*, 2025.

635 Youpeng Wen, Junfan Lin, Yi Zhu, Jianhua Han, Hang Xu, Shen Zhao, and Xiaodan Liang. Vid-  
 636 man: Exploiting implicit dynamics from video diffusion model for effective robot manipulation.  
 637 *Advances in Neural Information Processing Systems*, 37:41051–41075, 2024.

638

639 Hongtao Wu, Ya Jing, Chilam Cheang, Guangzeng Chen, Jiafeng Xu, Xinghang Li, Minghuan Liu,  
 640 Hang Li, and Tao Kong. Unleashing large-scale video generative pre-training for visual robot  
 641 manipulation. *arXiv preprint arXiv:2312.13139*, 2023.

642

643 Kun Wu, Chengkai Hou, Jiaming Liu, Zhengping Che, Xiaozhu Ju, Zhiqin Yang, Meng Li, Yinuo  
 644 Zhao, Zhiyuan Xu, Guang Yang, et al. Robomind: Benchmark on multi-embodiment intelligence  
 645 normative data for robot manipulation. *arXiv preprint arXiv:2412.13877*, 2024.

646 Youguang Xing, Xu Luo, Junlin Xie, Lianli Gao, Hengtao Shen, and Jingkuan Song. Shortcut  
 647 learning in generalist robot policies: The role of dataset diversity and fragmentation. *arXiv preprint  
 648 arXiv:2508.06426*, 2025.

648 Jianke Zhang, Yanjiang Guo, Xiaoyu Chen, Yen-Jen Wang, Yucheng Hu, Chengming Shi, and  
649 Jianyu Chen. Hirt: Enhancing robotic control with hierarchical robot transformers. *arXiv preprint*  
650 *arXiv:2410.05273*, 2024.

651 Jianke Zhang, Yanjiang Guo, Yucheng Hu, Xiaoyu Chen, Xiang Zhu, and Jianyu Chen. Up-vla: A  
652 unified understanding and prediction model for embodied agent. *arXiv preprint arXiv:2501.18867*,  
653 2025.

654 Qingqing Zhao, Yao Lu, Moo Jin Kim, Zipeng Fu, Zhuoyang Zhang, Yecheng Wu, Zhaoshuo  
655 Li, Qianli Ma, Song Han, Chelsea Finn, et al. Cot-vla: Visual chain-of-thought reasoning for  
656 vision-language-action models. In *Proceedings of the Computer Vision and Pattern Recognition*  
657 *Conference*, pp. 1702–1713, 2025.

658 Zhongyi Zhou, Yichen Zhu, Minjie Zhu, Junjie Wen, Ning Liu, Zhiyuan Xu, Weibin Meng, Ran  
659 Cheng, Yixin Peng, Chaomin Shen, et al. Chatvla: Unified multimodal understanding and robot  
660 control with vision-language-action model. *arXiv preprint arXiv:2502.14420*, 2025.

661 Brianna Zitkovich, Tianhe Yu, Sichun Xu, Peng Xu, Ted Xiao, Fei Xia, Jialin Wu, Paul Wohlhart,  
662 Stefan Welker, Ayzaan Wahid, et al. Rt-2: Vision-language-action models transfer web knowledge  
663 to robotic control. In *Conference on Robot Learning*, pp. 2165–2183. PMLR, 2023.

664

665

666

667

668

669

670

671

672

673

674

675

676

677

678

679

680

681

682

683

684

685

686

687

688

689

690

691

692

693

694

695

696

697

698

699

700

701

## A APPENDIX

## A.1 QUALITATIVE COMPARISON OF ENCODED FUTURE VISUAL REPRESENTATIONS

To qualitatively analyze the characteristics of different encoding methods, we visualize the features they produce. Specifically, we compare features from a single robot trajectory encoded in three ways: raw image pixels, continuous visual features from a ViT encoder, and discrete visual tokens from a VQ-GAN. We selected a trajectory from the Fractal dataset corresponding to the instruction *pick the coffee bag from the drawer onto the table*. For each frame, the resulting features—raw pixels (flattened from  $224 \times 224 \times 3$ ), ViT features (flattened from  $256 \times 1152$ ), and VQ-VAE tokens (2048-dim)—are first reduced to 50 dimensions via PCA and then projected into a 2D space using t-SNE for visualization.

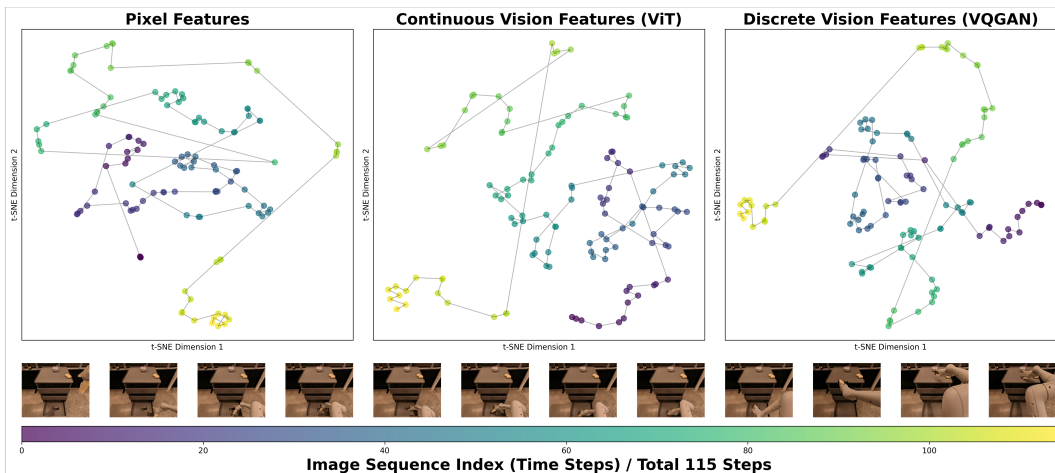


Figure 6: t-SNE Visualization of Different Future Representations.

Figure 6 illustrates the t-SNE visualizations for the trajectory encoded by these three methods. To highlight the temporal evolution, feature points from adjacent frames are connected by lines.

- **Pixel Features (Left):** This encoding preserves the most low-level information. We observe that despite small visual changes between consecutive frames, the corresponding pixel-level features exhibit high variance, often jumping into regions occupied by features from distant timesteps. This suggests that using raw pixel values as a predictive signal could mislead the policy by causing it to over-emphasize low-level, high-frequency changes.
- **ViT vs. VQ Features (Center and Right):** A comparison reveals a distinct “*circling phenomenon*” in the VQ-GAN visualization, where features from many different timesteps collapse into a dense central region. This indicates poor temporal separability in the context of manipulation trajectories. In contrast, the ViT features provide the best separation of the three methods, organizing features from different frames into distinct, minimally overlapping clusters.

This qualitative analysis supports our insight that continuous features, by virtue of focusing on high-level semantic information, serve as a more stable and suitable predictive signal for robot action policies within our framework.

## A.2 DETAILS ABOUT SIMULATION BENCHMARKS

**Calvin Benchmark** Calvin is a simulation benchmark designed for evaluating long-horizon, language-conditioned manipulation policies. It comprises four distinct environments (A, B, C, and D) and offers evaluation splits such as *ABC-D* and *ABCD-D*. In our experiments, we employ the *ABC-D* split to evaluate the single-view generalization capabilities of the models. Models are trained on data collected from environments A, B, and C, and subsequently evaluated in the unseen

756 environment D. This evaluation suite includes 34 different manipulation tasks organized into 1,000  
 757 long-horizon sequences, each of length 5. We report the average length of successfully completed  
 758 sub-task sequences.

760 **SimplerEnv Benchmark** SimplerEnv is a simulation benchmark designed to evaluate policies  
 761 trained on large-scale real-world datasets, such as Bridge-V2 and Fractal. It procedurally generates  
 762 scenes that mimic real-world environments using texturing techniques, allowing models trained on  
 763 real data to be tested directly in simulation without requiring physical deployment. The benchmark  
 764 supports two types of robot arms: the WindowX and the Google Robot. For our evaluation, we  
 765 conduct 240 runs for each task and report the average success rate.

### 767 A.3 DETAILS ON REAL WORLD EXPERIMENTS

#### 769 A.3.1 FRANKA PANDA ROBOT ARM

771 **Real-World Franka Emika Panda Arm** We deploy several models on a Franka Emika Panda  
 772 arm for real-world task comparison. The robot arm features 7 degrees of freedom (DoF). Its action  
 773 space is defined by a 7-dimensional vector, where the first six dimensions specify the relative change  
 774 in the end-effector’s 6D pose (3D position and 3D orientation), and the final dimension controls  
 775 the binary state of the gripper (open or closed). In our experiments, the policy takes images from  
 776 an on-board, first-person-view camera as visual input and outputs these relative actions. We first  
 777 collected a dataset of 2,000 trajectories spanning over 20 distinct tasks, encompassing six fundamental  
 778 skills: picking, placing, opening a drawer, closing a drawer, pressing a button, and routing a cable.  
 779 We evaluate performance on both seen and unseen task variations. The unseen category primarily  
 780 involves grasping novel objects not present in the training data.

781 The task suite for the Franka Panda arm includes:

- 783 • **Pick & Place:** Grasping and placing a variety of objects. The training set includes items  
 784 such as a toy banana, a toy eggplant, red/green/blue blocks, and red/yellow/black plates.
- 785 • **Press Button:** Pressing a toy button using a grasped black block as a tool.
- 786 • **Route Cable:** Routing a thin black rubber cable into a narrow slot.
- 787 • **Drawer Operation:** Opening a toy drawer.

790 **Unseen Tasks** These are designed to evaluate generalization: *Novel Objects*: Grasping objects not  
 791 seen during training (e.g., toy chili, toy strawberry, yellow block, large toy eggplant, arrow sticker,  
 792 marker pen). *Distractors*: Operating in the presence of irrelevant distractor objects. *Visual Variations*:  
 793 Adapting to changes in background color and object color.

794 We tested UniCoD, OpenVLA(Kim et al., 2024a), GR-1(Wu et al., 2023),  $\pi_0$  (Black et al., 2024),  
 795 UP-VLA (Zhang et al., 2025) and VPP (Hu et al., 2024) on this environment. The detailed results are  
 796 shown in Table 6 (corresponding to Figure 4).

798  
 799 Table 6: Detailed results on Franka-Emika Panda Robotarm. We evaluate each task 20 times (100  
 800 trials per skill) with random initialization and report the average success rate.

802 803 Model	804 Pick & Place		805 Press Button		806 Route Cable		807 Drawer		808 Avg Success	
	809 Seen	809 Unseen	809 Seen	809 Unseen	809 Seen	809 Unseen	809 Seen	809 Unseen	809 Seen	809 Unseen
OpenVLA	38	18	65	50	40	20	45	40	47	32
GR-1	45	32	80	60	50	50	60	40	59	46
UP-VLA	80	70	90	80	65	55	80	70	78	72
VPP	88	76	85	80	75	70	85	60	83	72
$\pi_0$	90	80	85	70	65	60	80	65	80	69
UniCoD (Ours)	<b>90</b>	<b>85</b>	<b>95</b>	<b>80</b>	<b>80</b>	<b>75</b>	<b>85</b>	<b>80</b>	<b>88</b>	<b>80</b>

810 A.3.2 XARM DEXTEROUS MANIPULATION  
811

812 **Real-World XArm with 12-DOF X-Hand** Our 12-DoF single-arm dexterous manipulation plat-  
813 form, which comprises a 7-DoF XArm and a 5-DoF hand, is controlled using a dual-view visual  
814 input from both first-person and third-person cameras. During evaluation, we test pick-and-place  
815 capabilities across 5 distinct task variations for a total of 50 trials. For all other skills, we conduct 20  
816 trials per task. The final performance is reported as the average success rate for each skill. We train  
817 different models using a dataset of 4,000 trajectories across more than 100 tasks. The models are  
818 then evaluated in a variety of seen and unseen scenarios, which cover 13 distinct skills, e.g., picking,  
819 placing, stacking, and pouring. To specifically test for visual generalization, we alter the background  
820 colors and novel objects during evaluation in the unseen scenarios.

821 The task suite for the XArm platform includes:

- 822 • **Dexterous Pick & Place:** Dexterously grasping and placing a wide range of objects. The  
823 training set includes a toy banana, a toy eggplant, a toy orange, small and large toy soccer  
824 balls, a computer mouse, a toy drawer, and more.
- 825 • **Move Cup:** Grasping and moving a cup to a different location.
- 826 • **Relocate:** Grasping an object and placing it adjacent to another target object.
- 827 • **Stack Cube:** Placing one block on top of another.
- 828 • **Pass:** Grasping an object and handing it to a human operator.
- 829 • **Press Button:** Directly actuating a toy button with a finger.
- 830 • **Unplug:** Extracting a rubber cable from a socket.
- 831 • **Drawer Operation:** Opening or closing a toy drawer.
- 832 • **Tool Use:** Using various tools, such as a spoon (e.g., for scooping) and a toy hammer (e.g.,  
833 for striking).

837 **Unseen Tasks** These are designed to evaluate generalization: *Novel Objects*: Grasping unseen  
838 objects and placing them to not-seen targets during training (e.g., apple, lemon, glass cup, glass  
839 plate, blue plate, toy kapibla, transparent plate, green apple, big ball, and various of novel objects).  
840 *Distractors*: Operating in the presence of irrelevant distractor objects. *Visual Variations*: Adapting to  
841 changes in background color and object color.

842  
843 Table 7: Detailed results on XArm with dexterous hand. We evaluate 50 times on Pick & Place tasks  
844 and 20 trials on other tasks with random initialization and report the average success rate.  
845

846 Model	847 Pick & Place		848 Move Cup		849 Relocate		850 Stack Cube		851 Pass	
	852 Seen	853 Unseen	854 Seen	855 Unseen	856 Seen	857 Unseen	858 Seen	859 Unseen	860 Seen	861 Unseen
848 OpenVLA	35	8	849 0	0	850 28	12	851 0	0	852 4	0
849 GR-1	40	10	850 0	0	851 16	12	852 0	0	853 0	0
850 VPP	69	35	851 64	40	852 70	66	853 64	44	854 48	32
851 $\pi_0$	65	45	852 50	28	853 75	56	854 45	40	855 40	35
852 UniCoD (Ours)	<b>75</b>	<b>73</b>	853 <b>75</b>	<b>45</b>	854 <b>83</b>	<b>78</b>	855 62	<b>50</b>	856 <b>50</b>	<b>40</b>
853 Model	854 Press Button		855 Unplug		856 Drawer		857 Tool Use		858 Avg Success	
	859 Seen	860 Unseen	861 Seen	862 Unseen	863 Seen	864 Unseen	865 Seen	866 Unseen	867 Seen	868 Unseen
865 OpenVLA	68	44	866 0	0	867 40	28	868 10	/	869 21	12
866 GR-1	64	40	867 0	0	868 48	24	869 20	/	870 21	16
867 VPP	96	88	868 <b>52</b>	20	869 72	56	870 <b>75</b>	/	871 67	48
868 $\pi_0$	95	90	869 45	30	870 <b>85</b>	75	871 42	/	872 60	50
869 UniCoD (Ours)	<b>97</b>	<b>95</b>	870 40	<b>35</b>	871 80	<b>77</b>	872 65	/	873 <b>70</b>	<b>62</b>

870 A.4 EXAMPLES OF DEMOS ON OOD-TASKS  
871

872 Examples of video on unseen objects are shown in Figure 7, where unseen objects are bold in the  
873 instructions. More demos can be found in our anonymous website.

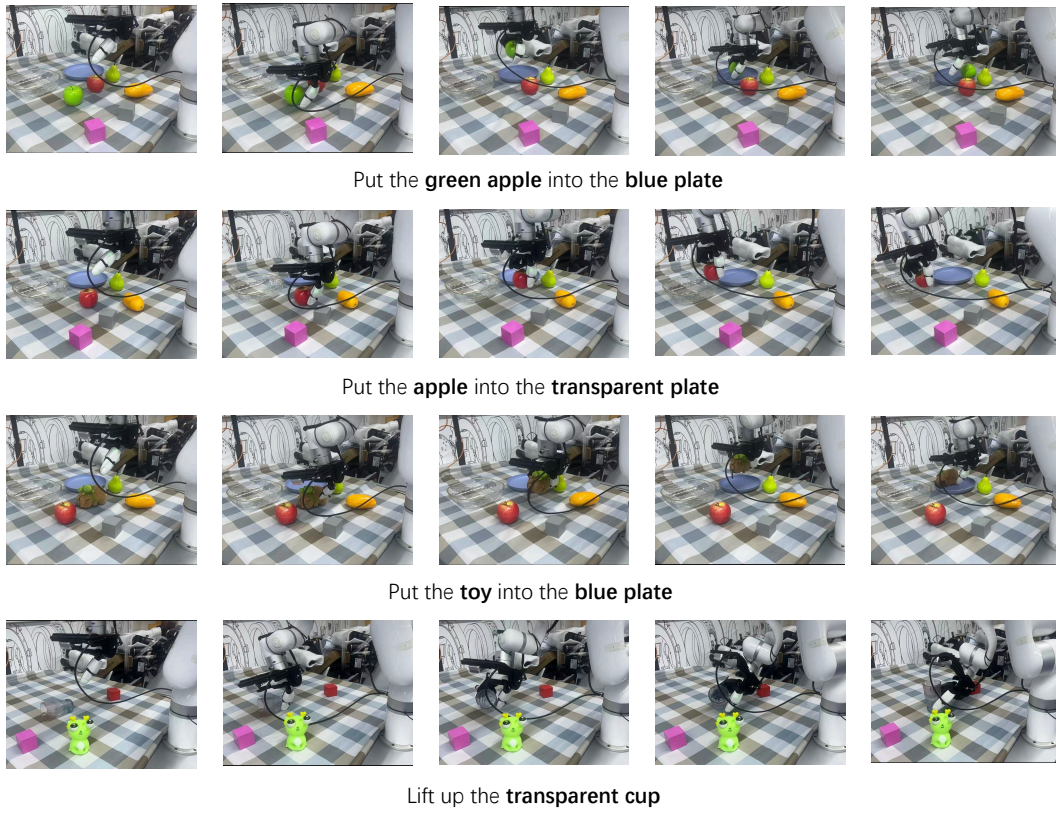


Figure 7: Examples of Semantic Generalization to OOD objects

### A.5 DATA USED FOR PRE-TRAINING

Table 8 summarizes the datasets employed during pre-training. To creating the robot vqa data, we employ Gemini 2.5(Comanici et al., 2025) to annotate text descriptions and task planning for a subset of video data. The RoboMind dataset inherently contains overall task descriptions and sub-tasks, which can be directly utilized as vision–language question–answer pairs.

Table 8: Datasets and the number of samples used for TI2E task and VQA task.

Task name	Dataset name	Number of samples
TI2E	AgibotWorld(Bu et al., 2025)	120k
	Galaxeal Open-World(Jiang et al., 2025)	99k
	Robomind(Wu et al., 2024)	20k
	Droid(Khazatsky et al., 2024)	76k
	Bridge(Walke et al., 2023)	55k
	Egodesk(Hoque et al., 2025)	320k
	Ego4D(Grauman et al., 2022)	500k
VQA	AgibotWorld VQA	120k
	Galaxeal Open-World VQA	99k
	Robomind VQA	20k
	Droid VQA	76k
	LLaVA-Pretrain(Liu et al., 2023)	558k

918 A.6 VQA DATA DESIGN  
919920 We present several examples of embodied VQA question–answer pairs in Figure 8.  
921

922  
923  
924  
925  
926  
927  
928  
929  
930  
931  
932  
933  
934  
935  
936  
937  
938  
939  
940  
941  
942  
943  
944  
945  
946  
947  
948  
949  
950  
951  
952  
953  
954  
955  
956  
957  
958  
959  
960  
961  
962  
963  
964  
965  
966  
967  
968  
969  
970  
971

Question: Based on current observations and instruction < Put apples, oranges and peaches in plastic bags. >, what subtask does the robot need to do next?

Answer: Next subtask is: place the held red apple into the plastic bag in the shopping cart.



Question: Based on current observations and instruction < Using the TV Remote. >, what subtask does the robot need to do next?

Answer: Next subtask is: Pick up the remote control from the table with left arm.



Question: Based on current observations and instruction < Stacking the blue, yellow, and orange cups. >, planning for the task the robot need to do?

Answer: Planning: Pick the blue cup; Place the blue cup on the yellow cup; Pick up the yellow cup; Place the yellow cup on the orange cup

Figure 8: Example of VQA.

For part of the embodied datasets (e.g., Agibot and RoboMIND), which contain precise instruction descriptions, we can directly construct QA pairs. For other datasets, we employ Gemini to decompose and annotate instruction descriptions according to the following prompt in Figure 9, 10.

## B USAGE OF LLMs

In the final stages of preparing this manuscript, the authors used a Large Language Model (LLM) solely for grammar checking and language polishing. The model assisted in improving sentence structure and correcting grammatical errors to enhance readability.

972  
973  
974  
975  
976  
977  
978  
979  
980  
981  
982  
983

**Prompt Example**

**System Message:**

```
"You are an expert in video analysis and robotic task
understanding.
You will be given an image sequence representing a video and a
reference
description. Your task is to decompose the total task into
several steps
which are needed to complete the task, and label each step with a
frame range."
```

**User Message:**

```
## Task Description
You will analyze an image sequence of a robotic arm performing a
specific task.
Your task is to make the overall task description more detailed
with the help of
the video clip, extract the necessary steps, and specify the
frame range for each step.

## Target
Step Extraction: Extract the key steps required to complete the
task. Each step includes:
- Specific actions decomposed from video and description
- Frame window: Specify the start and end frame for each step

## Requirements:
1. Different steps must correspond to different action types.
2. A step cannot contain two or more actions.
3. Two similar steps need to be merged into one.
4. The first step must start at frame 0, and the last step cannot
exceed {frame_num-1}.

## Output Format
Return output in JSON:
{
  "task_summary": "...",
  "steps": [
    {"step_description": "...", "start_frame": 0, "end_frame": 6},
    {"step_description": "...", "start_frame": 7, "end_frame": 12}
  ]
}

## Example Input
"task description": "Moving colored blocks into a container."
"video": image sequence with length {frame_num}
```

1013  
1014  
1015  
1016  
1017  
1018  
1019  
1020  
1021  
1022  
1023  
1024  
1025

1

Figure 9: prompt for Gemini.

```

1026
1027
1028
1029
1030
1031
1032
1033
1034
1035
1036
1037
1038     ## Example Output
1039     {
1040         "task_summary": "Moving the red and yellow blocks into a
1041                         container.",
1042         "steps": [
1043             {"step_description": "pick the red block.", "start_frame": 0,
1044                         "end_frame": 6},
1045             {"step_description": "place the red block into container.",
1046                         "start_frame": 7, "end_frame": 12},
1047             {"step_description": "pick the yellow block.", "start_frame":
1048                         13, "end_frame": 15},
1049             {"step_description": "place the yellow block into
1050                         container.", "start_frame": 16, "end_frame":
1051                         {frame_num-1}}
1052         ]
1053     }
1054
1055
1056
1057
1058
1059
1060
1061
1062
1063
1064
1065
1066
1067
1068             2
1069
1070
1071
1072
1073
1074
1075     Figure 10: prompt for Gemini.
1076
1077
1078
1079

```